International Journal of Engineering & Technology, 7 (4.39) (2018) 278-285

International Journal of Engineering & Technology

Website: www.sciencepubco.com/index.php/IJET

Research paper

Numerical Investigations on Fluid Flow and Solidification Behavior during Impact of a Hollow Molten Droplet on a Solid Substrate

Virendra Patel

Department of Mechanical Engineering Institute of Technical Education and Research Bhubaneswar, Odisha,
**Corresponding author E-mail: virendrapatel@soa.ac.in:*

Abstract

In thermal spraying coating process, powder materials are melted and driven towards the substrate's surface. This process involves impact of liquid droplet and its solidification. In the past studies it has been reported that central counter jet present in the hollow droplet impact on substrate. This counter jet affects total solidification time of splat and spreading pattern. The objective of the present work is to develop a two dimensional CFD model to investigate the effect of surface roughness during spreading and solidification of molten ZrO_2 hollow droplet impacting on a substrate of Stainless steel. The governing equations for fluid flow are solved numerically using a pressure-based finite volume method, following the SIMPLE algorithm presented by Patankar (1980). To track droplet THINC/WLIC method is used which is a VOF (Volume of Fluid) type method. To model surface tension force, the CSF (continuum surface flow) model is used. Enthalpy-based formulation is used to solve energy equation.

Keywords: *Hollow droplet impact; solidification*

1. Introduction

Molten metal droplet solidification on a cold substrate is common in many manufacturing processes like, micro droplet soldering, Atomization, thermal spray deposition, melt spinning, laser surface melting. Among the above process, thermal spraying process is widely used in industry to develop functional coating, e.g. wear and corrosion resistant. In plasma spraying, ceramics powders are injected into a plasma torch where they are heated, melted, and driven towards the surface of a substrate. The main advantage of YSZ powders made up by hollow particles is that, particles undergoes complete melting, with the temperature being quite uniform across the particle. The surface temperature of hollow particles is close to their mean-mass temperature, enabling more correct experimental data regarding the splat and coating formation process

Significant studies [1–7] are being devoted to study solidification behavior of the droplet impact process. S.D. Aziz, S. Chandra [1] has studied the impact and solidification of molten tin droplets on a stainless steel surface. They observed the formation of fingers on the periphery of the droplet.S. Shakeri, S. Chandra [2] reported that thermal contact resistance is proportional surface roughness. At higher surface roughness, heat transfer from the droplet to the substrate is found to reduce, delaying the onset ofsolidification and reducing splashing.S. Kamnis, S. Gu[3]has reported that air entrapment in splat, spreading, solidification behavior are dependent to surface roughness. S. Kamnis, S. Gu, T.J. Lu, C. Chen [4] developed numerical modelling of the dynamics of transient flow during the impact process, to study spreading, break-up, air entrapment and solidification of droplet. H. Tabbara, S. Gu [5] simulated the transient flow of a liquid metal droplet impacting, to study the deformation and solidification behavior on a solid substrate. They describe in detail how the solidification process varies with an increasing impact velocity.H.Safaei, and Emami[6] have reported that the spreading and solidification behavior of a completely molten droplet is quite different from a semi-molten droplet during impact process.D. Li, X. Duan, Z. Zheng and Y. Liu [7] have reported that impact behaviors of the hollow droplet are different from a continuous dense droplet. They also found that heat transfer during impact of hollow droplet is lower than that during dense droplet impact.A Kumar, Sai Gu and S Kamnis[8] have reported that low impact speed delayed the rupture of the droplet shell. They also reported that larger impact velocity is reason for faster growth of the counter jet**.**In other studiesA Kumar, Sai Gu, H Tabbara, and S Kamnis[9] have reported that in case of hollow droplet, central splash is more as compared to dense droplet. Final spreading diameter is smaller, and splat thickness is more for the hollow droplet. Total solidification time of splat is much larger for hollow droplet impact.In all these studies of droplet impact [1–7], assume that the droplets are continuous and dense. A very limited work [8-9] are related to impact of hollow droplet. The detailed study of impact of hollow droplet and solidification behavior on a cold substrate is missing. The limited studies in this field [10,11] reported that coating done with hollow particles opens up improved coating properties. The thermal insulation property of a surface can be enhanced by controlling the porosity of coating [11-12]. The voids in droplet influence not only hydrodynamic and solidification behavior but it also influences the particle in flight behavior such as acceleration, and oxidation [13].

This work reports modelling of the solidification and spreading during impact of hollow liquid droplet onto a solid flat surface. The detailed studies of effect of surface roughness on spreading, solidification and formation of splat is done.

2. Mathematical Formulation

2.1 Numerical Modeling

Numerical simulation of liquid metal droplets impacting on cold substrate is a challenging proposition. The complexities include the free surface deformation, both mode of heat transfer convective and diffusive and presence of solid/liquid phase-change boundary in solidification. Various methods are employed to track the free surface evolution such as volume tracking methods, front tracking methods, level set methods, phase-field formulations, continuum advection schemes, boundary integral methods and moving mesh methods. Due to the rapid deformation of the droplet during the impact process, both convective and diffusive energy transfers are important and due to this it is included in the energy equation. The modeling of a phase change shares many of the difficulties of the free surface. It also requires the accounting of the latent heat of fusion in the energy equation.
In this work the VOF model is used to track interface between the droplet and the air by assuming immiscible fluids. The momentum equation is used for air and droplet not for substrate. The energy equation is solved for whole domain. Surface tension at free surfaces is modeled using the continuum surface force (CSF) model [14]. SIMPLE method is used to solve discretized energy and momentum, a method in which the pressure Poisson equation (PPE) is solved. The existence of phase change in the numerical calculations poses a challenge because it is a mathematical discontinuity. There are two popular approaches to the solution of this problem: The Stefan approximation, it predicts the precise location of the solid/liquid interface and, the enthalpy method, used when the phase-change front is known to occur within a known interval. Stefan approximation requires the use of a deforming grid or transformed coordinate system. The enthalpy formulation allows a fixed grid to be used in the solution. Also, it removes the need to explicitly satisfy conditions at the phase-change front, thus making it suitable for use in standard solution procedures.

2.2 Assumptions

In the modeling of impingement of molten droplets, the following assumptions and approximations are made:

- The droplet is assumed to be initially spherical. Deformation in the droplet as it is accelerated towards the substrate is considered to be negligible since the size of the droplets is small (of the order of μm).
- The droplet and air interface is assumed to be adiabatic, i.e. the free surface is insulated from the ambient, and the radiation mode of heat transfer are neglected.
- The variation of material properties such density and viscosity are modeled as independent of the temperature.
- The thermal and fluid properties of the droplet material in solid and liquid states are different except density.
- The value of thermal contact resistance and contact angle is constant for the entire simulation.

2.3 Governing Equations

The numerical scheme in the flow solver used in this study is based on a finite volume method. The continuum formulation based on the classical mixture theory [15-17] is adopted for modelling the solidification in the droplet.. A cell may consist of both droplet material and air. Material properties in different cell is based on Volume-fraction-averaged, that is given as:

$$\rho = F\rho_d + (1-F)\rho_{air} \tag{2.3a}$$

$$k_{eff} = Fk_d + (1-F)k_{air} \tag{2.3b}$$

$$c_{eff} = Fc_d + (1-F)c_{air} \tag{2.3c}$$

$$\mu_{eff} = F\mu_d + (1-F)\mu_{air} \tag{2.3d}$$

VOF equation:

$$\frac{\partial F}{\partial t} + \nabla\cdot\left(\vec{u}F\right) - F\nabla\cdot\vec{u} = 0 \tag{1}$$

Continuity equation:

$$\nabla\cdot\left(\vec{u}\right)=0 \tag{2}$$

Momentum conservation:
In a single pressure system as considered in the VOF method [18], the normal component of the pressure gradient at a stationary inclined solid wall must be different for each phase. To simplify the problem of boundary condition, a modified pressure is defined as

$$P_{-\rho gh} = P - \rho\vec{g}\cdot\vec{x} \tag{3}$$

Using Eq. (3) the momentum equation is rearranged [18] as:

$$\frac{\partial}{\partial t}(\rho\vec{u}) + \nabla\cdot(\rho\vec{u}\vec{u}) = -\nabla P_{-\rho gh} + \nabla\cdot\left[\mu(\nabla\vec{u}+\nabla\vec{u}^T)\right] - \vec{g}.\vec{x}\nabla\rho + F_{vol} - S\vec{u} \tag{4}$$

Where F_{vol} is continuum surface tension force (CSF) model (Brackbill et al., 1992) which has been discussed in section 2.4 and

$$S = \begin{cases} \left[C\dfrac{(1-f_l)^2}{f_l^3+e}\right] for F = 1 \\ 0 for F < 1 \end{cases} \tag{5}$$

The value of constant *C*is taken as150,000 kg/m^{3}s^1 in the current model [15]. A constant value of contact angle θ of 90°has been considered based on the study reported in [19-21]. It was reported that the effect of dynamic contact angle on the droplet spreading becomes less important for droplet in actual thermal spray conditions where $We \gg Re^{\frac{1}{2}}$ [22]
Energy conservation:

$$\frac{\partial}{\partial t}(\rho c_{eff} T) + \nabla\cdot(\rho\vec{u}\, c_{eff} T) = \nabla\cdot(k_{eff}\nabla T) + S_h \tag{6}$$

Where

$$S_h = \begin{cases} -\left[L_d\dfrac{\partial}{\partial t}(\rho f_l)\right] for F = 1 \\ 0 for F < 1 \end{cases} \tag{7}$$

The latent heat associated with phase change is incorporated in source term Sh[9,23] of energy equation that is related to liquid fraction of cell. The methodology to calculate the liquid fraction is given in section 2.5. Thermal contact resistance is taken in the range of 10^{-6}–10^{-8} m^2 K/W [24-26].

2.4 Surface Tension Force Model

The continuum surface tension force, $F_{vol}$is calculated using the standard method of Brackbill et al. [27],

$$F_{vol} = \sigma\kappa(\vec{x})\frac{\rho}{\rho_d + \rho_{air}}\nabla F \quad (8)$$

2.5 Liquid Fraction Calculation

In equilibrium solidification liquid fraction (f_l) are calculated using enthalpy porosity method. It is an iterative method described below.

$$f_l = \frac{\Delta H}{L} \quad (9)$$

In the present work, an iterative updating scheme to update latent heat content, as detailed in [16], is implemented. It is given as.

$$\left[\Delta H_P\right]_{n+1} = \left[\Delta H_P\right]_n + \frac{a_p}{a_p^0}\lambda\left[\left\{h_p\right\}_n - G^{-1}\left\{\Delta H_P\right\}_n\right] \quad (10)$$

In Eq. (10), $a_p^0 = \rho\Delta V/\Delta t$ and a_p is the coefficient of the nodal temperatureT_P in the discretization equation of the energy equation. G^{-1} for solidification of pure substance is given as [16]

$$G^{-1}\left[\Delta H\right] = c_d T_m \quad (11)$$

The value of relaxation factor (λ ~ 0.3–0.7) is taken in order to get converged and stable solutions.

3. Problem Setup

3.1 Model Description

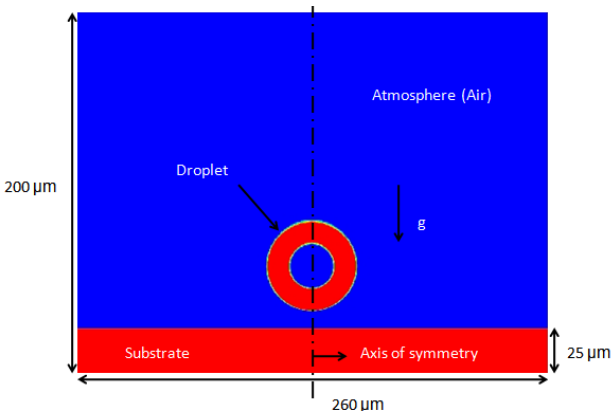

Figure 3.1: Schematic of droplet impact on a substrate

Figure 3.1 shows the geometry of our problem and initial condition. We modeled using 2D axis symmetric model. A spherical liquid ZrO_2 hollow droplet of outer diameter D_o and inner diameter of D_i with initial temperature T_d impact at a prescribed impact speed V m/s onto to a solid substrate of Stainless steel at a normal incidence.

3.2Boundary Conditions

In Fig. 3.2 Wall 1 is axial symmetry of the domain as our model is 2D axis symmetry. Since droplet is falling in downward direction, so wall 2 is pressure inlet and wall 3 is pressure outlet. Wall 4, 5 and 6 are the surface of substrate. Boundary 7 is air droplet interface.

Table 3.1: Boundary conditions

Boundary	Navier-Stokes equations	Heat transfer equation
1	Axial symmetry	Axial symmetry
2	Pressure outlet	In flow
3	Pressure outlet	Out flow
4	No slip	Conjugate
5,6	No slip	Temperature
7	Interface	adiabatic

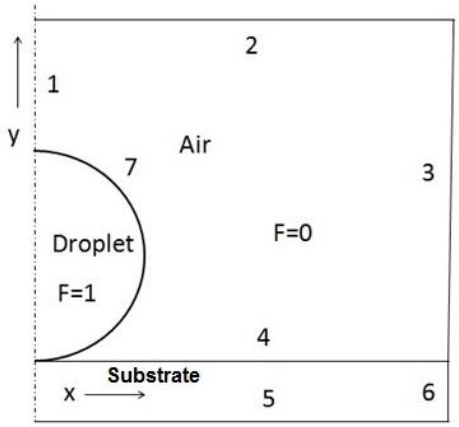

Figure 3-2: Initial configuration of droplet. Number from 1-6 show different walls and their boundary conditions are shown in Table 3.1

3.3 Material Properties Data

Table 3.1:

Impinging droplet material	Zirconia (ZrO_2)
Substrate material	Stainless steel (SS)
Gas phase	Air
Droplet initial temperature	3000 K
Substrate initial temperature	300 K
Solidification temperature (ZrO_2)[30]	2950 K
Density (solid ZrO_2) [30]	5890 kg/m3
Density (liquid ZrO_2)	5700 kg/m3
Thermal conductivity (SS)	14.9 W·m−1/K
Thermal conductivity (solid ZrO_2) [30]	2.32 W·m−1/K
Thermal conductivity (liquid ZrO_2) [30]	2.00 W·m−1/K
Thermal conductivity (air)	0.0242 W·m−1/K
Contact angle [41]	90°
Density (SS)	7900 kg/m3
Density (air)	1.225 kg/m3
Viscosity (air)	1.7894×10−5 kg·m−1/s
Viscosity (liquid ZrO_2) [29]	0.021 kg·m−1/s
Droplet surface tension [29]	0.43 N/m
Specific heat capacity (ZrO_2) [29]	713 J·kg−1/K
Latent heat of fusion [30]	7.07×105J/kg
Specific heat capacity (SS)	477 J·kg−1/K
Specific heat capacity (air)	1006.43 J·kg−1/K1

3.4 Validation of Model

Numerical simulation is performed for impact of glycerin hollow droplet of. Free surface evolution and counter jet in simulation using the numerical code has been validated qualitatively against a standard bench-mark experimental result [28].

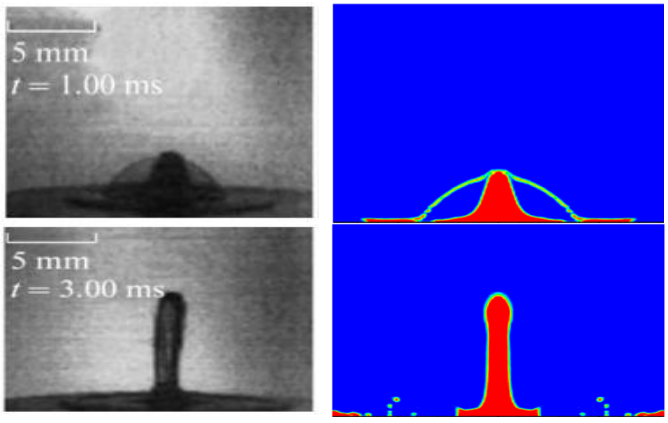

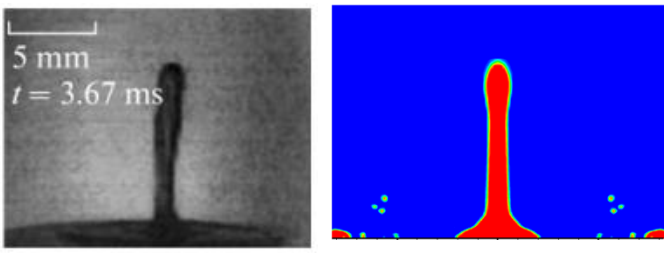

(a) (b)

Figure 3-3: Comparison of (**a**) the experimental [28] and (**b**) simulated hollow droplet impact behavior on the solid surface

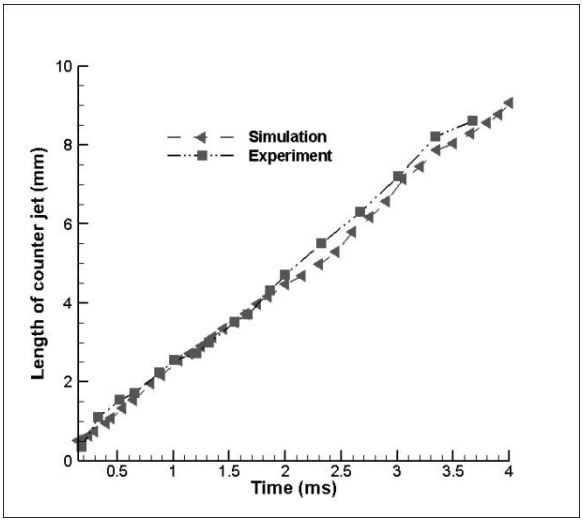

Figure 3-4: The comparison of evolution of the counter jet length with experimental result [28]

This is 2-D axisymmetric problem. In the experiment [28], hollow droplet of glycerin was made to impact on a solid and length of counter jet was investigated. We have simulated this problem using FORTRAN code. Figures 3-3 (a) and 3-3 (b) shows that the predicted impact behavior is matching with the experimental result [28]. Evidently, the rupture of the droplet shell (1.0 ms) predicted in current simulation is similar to the experiment. The instantaneous length the counter jet is also very much similar with the experiment that is shown in figure 3-4.

4. Results and Discussions

4.1 Solidification Behavior of Dense Droplet and Hollow Droplet

After validating model numerical, simulation of solidification of hollow droplet and dense droplet of ZrO_2 impacting on cold substrate of stainless steel are done with initial condition given in the Table 4.1.

Table 2: 1Initial conditions

Parameter	Value(in SI unit)
Initial temperature of drolet	3000 K
Outer Diameter of droplet	50 µm
Inner Diameter of droplet	25 µm
Impact speed	100 m/s
Substrate temperature	300 K

Undercooling is not considered at solid/liquid interface. It assumed that as the temperature of liquid metal reaches to equilibrium freezing temperature(T_M) it starts solidifying. The value of heat transfer coefficient for this case is taken as $h = 1\times10^7 W/m^2 K$.

Figure 4.1 shows snapshots for spreading and solidification of the dense droplet and hollow droplet at different time. A similar spreading and solidification behaviour of a dense droplet and hollow droplet impacting on a substrate is observed as reported in [9]. In both case solidifications start at same time that is 0.2 µs that is clear in figure 4-4, but at later time solid liquid interface growth is faster in the case of hollow droplet this is because of presence of counter jet. It can be also seen that the spreading ratio (defined as ratio of maximum spreading diameter to droplet initial diameter) for the case of hollow droplet is lower than that of dense droplet. This is because, in the case of hollow droplet, due to counter jet some part of liquid come toward axis while other part goes away from axis. But for the case of dense droplet liquid is continued to go away from the axis. The dense droplet solidifies completely at about 5.4 µs and in the case of hollow droplet it takes more than 30 µs as counter jet takes time to come back on substrate. It can be observed from the Figure 4- 1 that evidently, the predicted rupture of the droplet shell (1.2 µs) in case of hollow droplet. Recoiling can be also seen in case of hollow droplet at time 2.2 µs but in case of dense droplet it can be seen at time 2.5 µs.

In case of hollow droplet more air entrapment occurs due to rupture of the droplet shell due to counter jet. Solidification is at faster rate in case of hollow because of counter jet due to this thickness is larger as compared to dense droplet solidification, where no counter jet is present at any instant of time which promote more splashing.

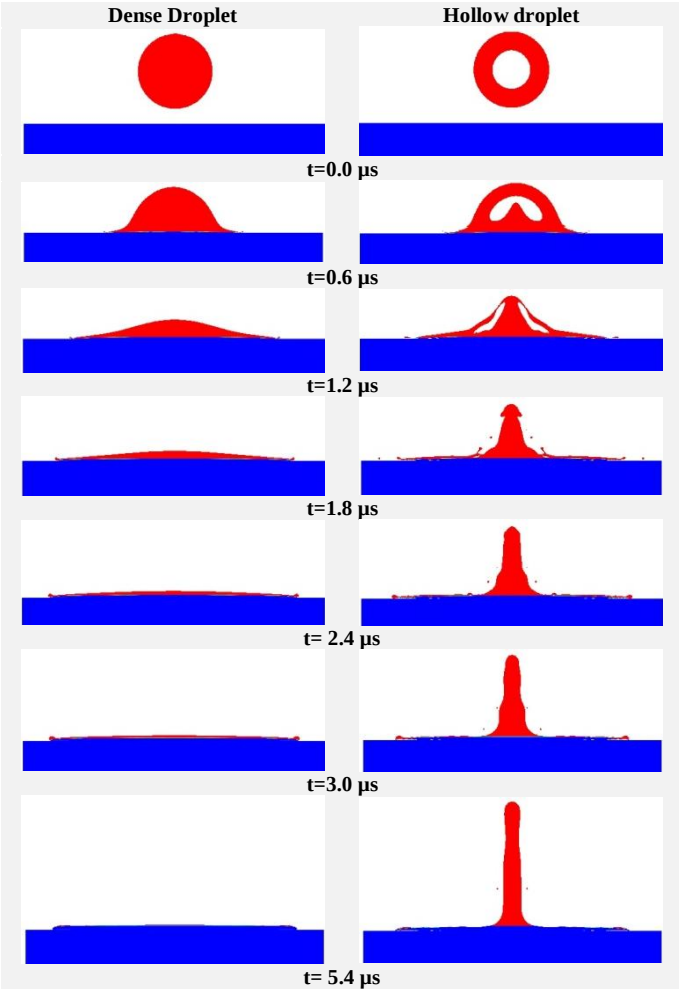

Figure 4: 1liquid fraction distribution at different time instant for the case of dense and hollow droplet

Figure 4-2 shows the time evolution of droplet bottom temperature. It can be seen that before the start of solidification the temperature decreases as the heat is transfer from the liquid to solid substrate. But after solidification begins, the temperature is constant in case of dense droplet for very short interval of time,

this is due to release of latent heat during solidification, its due to slow solidification rate as compared to hollow droplet, but in case of hollow droplet it is not observed its due high heat transfer rate. In case dense droplet latent heat released is transferred to substrate while it is transferred to substrate as well as in counter jet in case of hollow droplet. After this the temperature of the newly solid deposit at the substrate/droplet interface decreases for some time after that it is almost constant until the whole droplet solidified. In case of hollow droplet cooling rate is higher as compared to dense droplet, it's because the latent heat is transferred to substrate as well as in counter jet in case of hollow droplet.

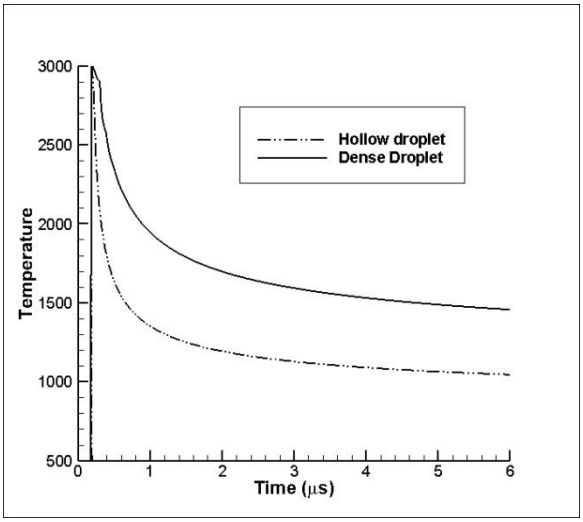

Figure 4-2: Temperature history near the substrate

Figure 4-3 compared the solid- liquid interface speed for the case of dense droplet and hollow droplet. It can be observed that initially the interface speed is same for the hollow droplet and dense droplet case. As the time progress its value for the case of hollow droplet is higher due to occurrence of counter jet and then again is almost same as the case of dense droplet. In the initial time in case of hollow droplet, interface speed is governed by cooling rate due heat transfer in to substrate but as time progresses interface speed is governed by cooling rate due heat transfer in to substrate as well as released latent transferred to counter jet in case of hollow droplet. But in case of dense droplet, interface speed is governed by cooling rate due heat transfer into substrate only.

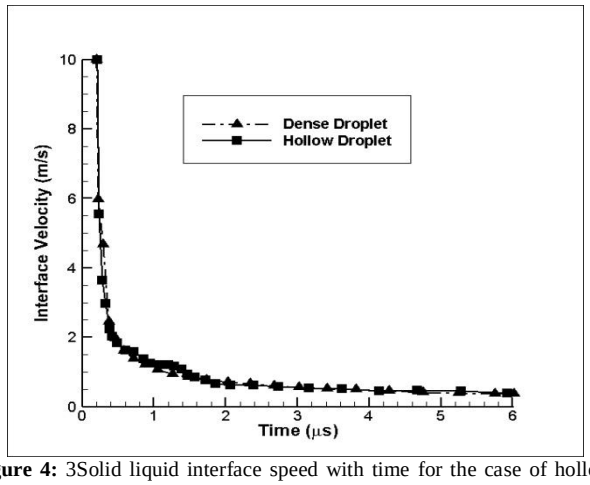

Figure 4: 3Solid liquid interface speed with time for the case of hollow droplet and dense droplet

Figure 4-4 shows solid-liquid interface position (solidified thickness) near the axis with time for the hollow droplet and dense droplet case. As the droplet is above the substrate, it first come to substrate then start solidify, it can be observed from figure 4-4 that solidification starts at time 0.2 μs for both the case. It can be seen that the solid-liquid interface is at same position for both case. But after time 0.4 μs the solid-liquid interface for the case of hollow droplet is ahead. It can be concluded that occurrence of counter jet in the case of hollow droplet caused the higher solid-liquid interface growth by taking some part of latent heat released during solidification. Solidified thickness is always higher in case of hollow droplet due to occurrence of counter jet.

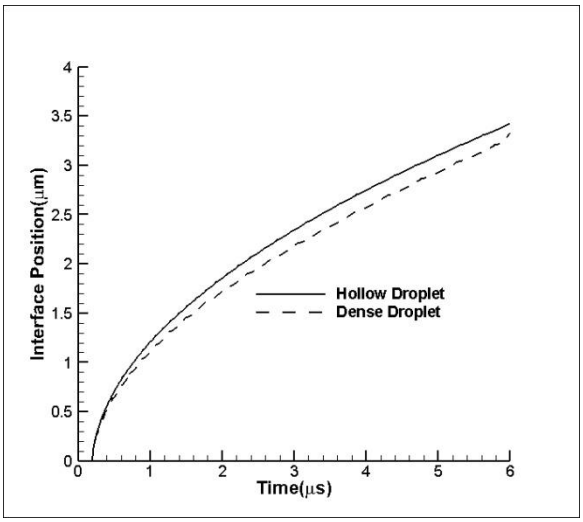

Figure 4-4: Interface position from substrate surface with time for the case of hollow droplet and dense droplet

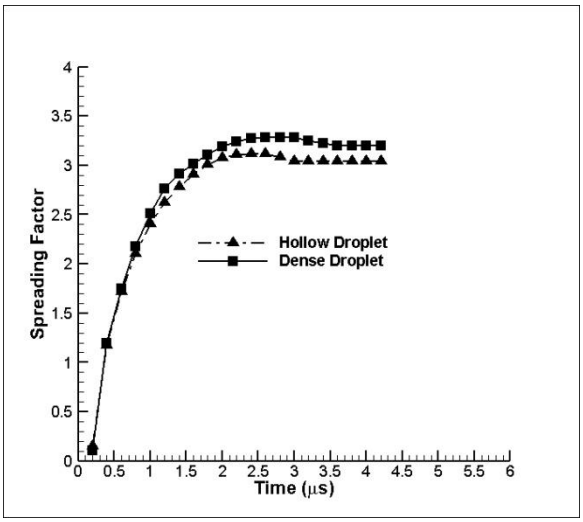

Figure 4-5: Spreading factor with time for the case of hollow droplet and dense droplet

Figure 4-5 shows the spreading ratio variation with time of both the case hollow droplet and dense droplet. The graph shows that the spreading ratio in the case of dense droplet is higher in comparison of the case of hollow droplet. Due to occurrence of counter jet during hollow droplet impact some part of liquid in the cell impacting on substrate goes towards axis and other part goes toward periphery. While in case dense droplet whole liquid before solidification goes towards periphery. In this way more liquid goes towards periphery in case of dense droplet in compared to case of hollow droplet. That causes higher spreading ratio for case of dense droplet. For the present case the maximum spreading factor is nearly 3.3 in case of dense droplet and 3.1 for the hollow droplet impact.

4.2 Effect of Interfacial Heat Transfer Coefficient

In this section, effect surface heat transfer coefficient of substrate on different parameters for hollow droplet is plotted and related

physics are described. Surface roughness is accounted at thermal convective resistance at droplet substrate interface. In these cases, impact speed was 100 m/s.

Figure 4.6 shows the variations of temperature with time at a bottom point in the droplet which is just above the substrate surface with different heat transfer coefficient. This graph shows comparison of cooling curve for the different heat transfer coefficient ($5x10^7$ W/(m^2K) and $5x10^6$ W/(m^2K)). It can be seen that at higher heat transfer coefficient cooling rate is more as a results interface velocity is high.

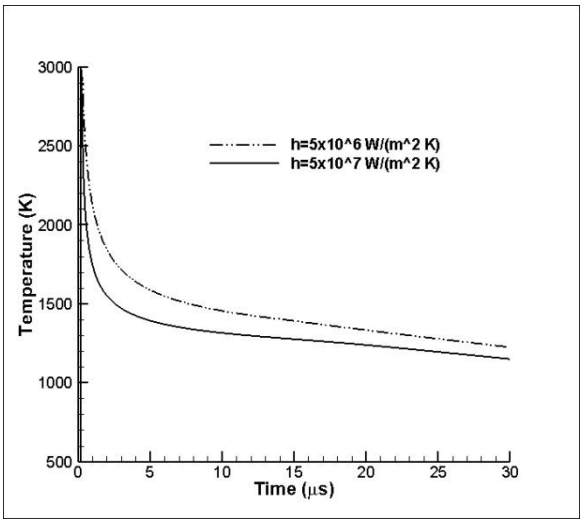

Figure 4-6: Temperature history with time near the substrate for different heat transfer coefficient

Figure 4-7 shows the interface position at different heat transfer coefficient. It can be observed that interface position is higher up to time 12 μs for the case of higher heat transfer coefficient as compared to lower heat transfer coefficient. The reason behind this is that at higher heat transfer coefficient heat transfer from the droplet to substrate is high as a results interface velocity is high and interface growth will be high. But after time 12 μs interface position is ahead for the case of lower heat transfer coefficient. Solidification happens only at neck and latent heat released at this point of time defuse very fast. So solidification rate suddenly gets accelerated and interface velocity increases, it can be seen in figure 4-8. But this effect for higher heat transfer coefficient is seen about 15 μs. For higher heat transfer coefficient solidification rate is high and it arrest the counter jet and it delayed the phenomenon of thinning of neck of counter jet.

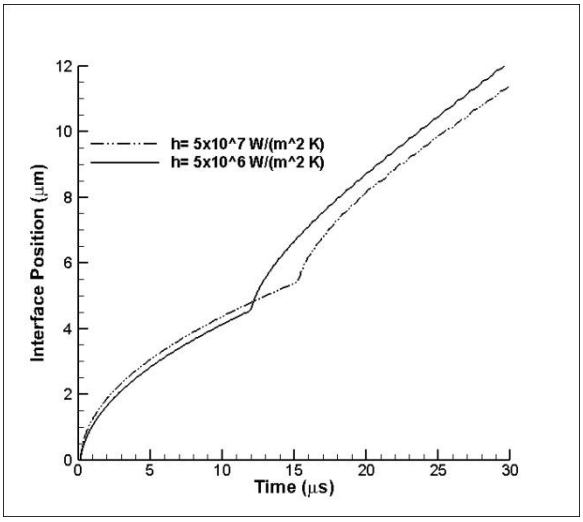

Figure 4-7: Interface position from substrate surface with time for different heat transfer coefficient

Figure 4-8 shows the interface velocity and corresponding interface temperature for different heat transfer coefficient. It coefficient because at higher heat transfer coefficient heat transfer will be high as a results cooling rate will be more. Higher cooling rate will cause higher interface speed. The reverse is true for the lower heat transfer coefficient.

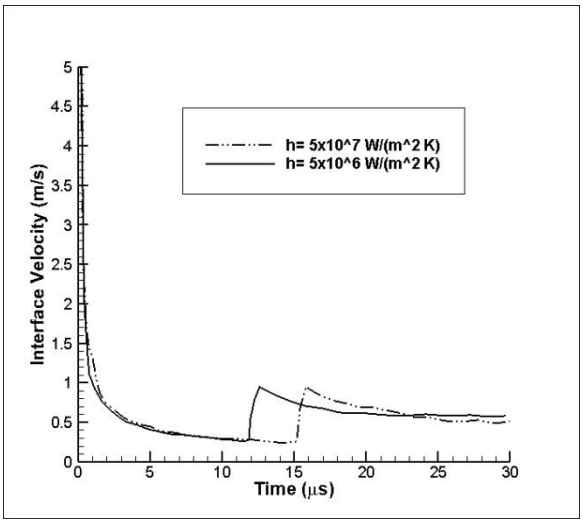

Figure 4-8: Solid liquid interface speed with time for different heat transfer coefficient

Figure 4-9 shows the comparison of length of counter jet for different heat transfer coefficient. It is noted that at lower heat transfer coefficient length of counter jet is higher. At higher heat transfer coefficient initially solidification rate is higher which arrest the counter jet. At lower heat transfer coefficient solidification rate is slow and it allows to counter jet to grow at faster rate.

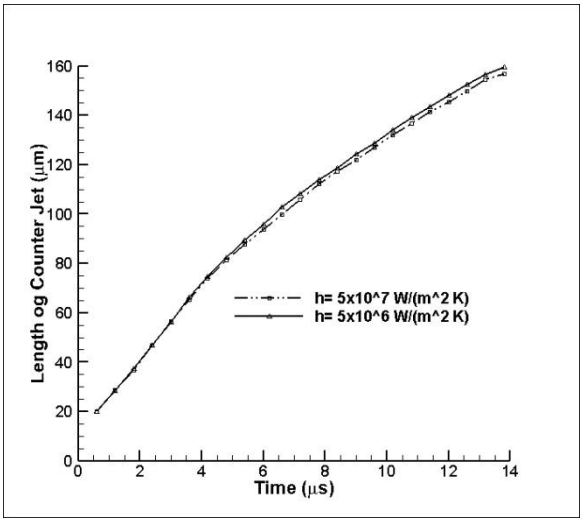

Figure 4-9: Length of counter jet with time for different heat transfer coefficient

Figure 4-10 shows the comparison of spreading factor for different heat transfer coefficient. It is to be noted that at lower heat transfer coefficient spreading factor will be high. At lower heat transfer coefficient solidification is slow and liquid at periphery get more time to travel and it causes higher spreading factor. At higher heat transfer coefficient temperature reaches to the freezing temperature very fast as results solidification started early which offer hindrance in the spreading which causes less spreading factor.

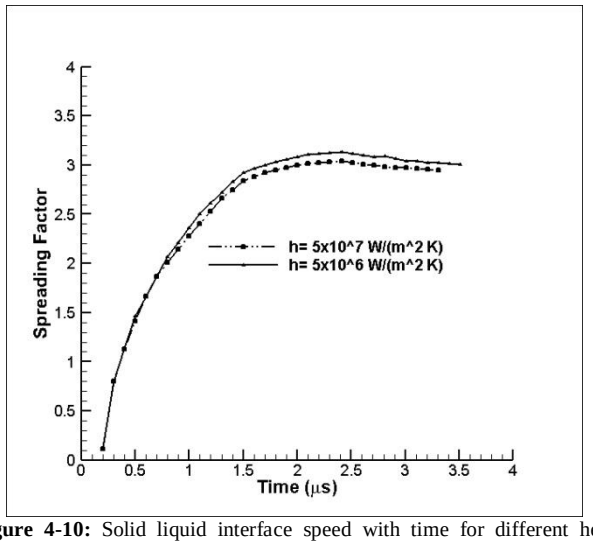

Figure 4-10: Solid liquid interface speed with time for different heat transfer coefficient

5. Conclusion

This study, detailed study of solidification behaviour and spreading pattern of hollow droplet impacting on cold substrate and quantitative comparison with dense droplet has done.The results predicted from the present model are very much similar to the experimental results and well validated. The hollow droplet impact results more uniform and a thicker splat as compared to the analogous continuous droplet. Spreading and solidification behavior is very different in case of hollow droplet and dense droplet which affect the splat morphology. Cooling rate near the substrate surface and solidification rate is higher for the case of hollow droplet. The solidification time for the splat formed with hollow droplet is also relatively large. Effect of heat transfer coefficient on various parameter (spreading ratio, interface velocity, interface temperature, interface position) has been studied. At higher heat transfer coefficient length of counter jet and spreading factor is less.

References

[1] S.D. Aziz, S. Chandra, Impact, Recoil and Splashing of Molten Metal Droplets, Int. J. Heat Mass Transfer 43 (2000) 2841.

[2] S. Shakeri, S. Chandra,Splashing of molten tin droplets on a rough steel surface, Int. J. Heat Mass Transfer 45 (2002) 4561.

[3] S. Kamnis, S. Gu,Numerical modelling of droplet impingement, J. Phys. D: Appl. Phys. 38 (2005) 3664.

[4] S. Kamnis, S. Gu, T.J. Lu, C. Chen, Numerical modelling of sequential droplet impingements, J. Phys. D: Appl. Phys. 41 (2008) 165303 (7 pp.).

[5] H. Tabbara, S. Gu, Modelling of impingement phenomena for molten metallic droplets with low to high velocities, Int. J. Heat Mass Transfer 55 (2012) 2081.

[6] H. Safaei and M. EmamiNumerical comparison between the impact of a completely molten and a semi-molten hollow droplet on a surface MME 2017, 17(8): 267-278.

[7] D Li, X Duan, Z Zheng, and Y Liu, Dynamics and heat transfer of a hollow droplet impact on a wetted solid surface, International Journal of Heat and Mass Transfer122, (2018) 1014-1023.

[8] A Kumar, Sai Gu, S Kamnis, Simulation of impact of a hollow droplet on a flat surface, ApplPhys A (2012) 109:101–109.

[9] A Kumar, Sai Gu, H Tabbara, S Kamnis, Study of impingement of hollow ZrO2 droplets onto a substrate, Surface & Coatings Technology 220 (2013) 164–169.

[10] O.P. Solonenko, I.P. Gulyaev, A.V. Smirnov, Plasma processing and deposition of powdered metal oxides consisting of hollow spherical particles, Tech. Phys. Lett. 34 (2008) 1050.

[11] K. Shinoda, H. Murakami, Splat Morphology of Yttria-Stabilized Zirconia Droplet Deposited Via Hybrid Plasma Spraying, J. Therm. Spray Technol. 19 (2010) 602.

[12] M.P. Planche, S. Costil, C. Verdy, C. Coddet, Different spray processes for different Al_2O_3 coating properties, Appl. Phys. A: Mater. Sci. Process. 99 (2010) 665.

[13] S. Kamnis, S. Gu, M. Vardavoulias, Numerical Study to Examine the Effect of Porosity on In-Flight Particle Dynamics, J. Therm. Spray Technol. 20 (2011) 630.

[14] S. Sampath, X.. Jiang, J. Matejicek, A.. Leger, A. Vardelle, Substrate temperature effects on splat formation, microstructure development and properties of plasma sprayed coatings Part I: Case study for partially stabilized zirconia, Mater. Sci. Eng. A. 272 (1999) 181–188.

[15] S. Kamnis, S. Gu, Numerical modelling of droplet impingement, J. Phys. D. Appl. Phys. 38 (2005) 3664–3673.

[16] N. Pathak, A. Kumar, A. Yadav, P. Dutta, Effects of mould filling on evolution of the solid-liquid interface during solidification, Appl. Therm. Eng. 29 (2009) 3669–3678.

[17] W.D. Bennon, F.P. Incropera, A continuum model for momentum, heat and species transport in binary solid-liquid phase change systems-I. Model formulation, Int. J. Heat Mass Transf. 30 (1987) 2161–2170.

[18] Ubbink, H. Computational Fluid Dynamics of Dispersed Two-Phase Flows at High Phase Fractions,Ph.D Thesis, Imperial College of Science, Technology and Medicine, London, 2002.

[19] M. Pasandideh-Fard, Y.M. Qiao, S. Chandra, J. Mostaghimi, Capillary effects during droplet impact on a solid surface, Phys. Fluids. 8 (1996) 650–659.

[20] M. Pasandideh-Fard, J. Mostaghimi, On the spreading and solidification of molten particles in a plasma spray process : effect of thermal contact resistance, Plasma Chem. Plasma Proccssing. 16 (1996) 83–98.

[21] M. Xue, Y. Heichal, S. Chandra, J. Mostaghimi, Modeling the impact of a molten metal droplet on a solid surface using variable interfacial thermal contact resistance, J. Mater. Sci. 42 (2007) 9–18.

[22] M. Pasandideh-Fard, M. Qiao, S. Chandra, and J. Mostaghimi, Capillary Effects During Droplet Impact on a Solid Surface, Phys. Fluids.8(3) (1996) 650-659.

[23] A.D. Brent, V.R. Voller, K.J. Reid, Enthalpy-porosity technique for modeling convection-diffusion phase change: application to the melting of a pure metal, Numer. Heat Transf. 13 (1988) 297–318.

[24] H. Zhang, X.Y. Wang, L.L. Zheng, S. Sampath, Numerical simulation of nucleation, solidification, and microstructure formation in thermal spraying, Int. J. Heat Mass Transf. 47 (2004) 2191–2203.

[25] H. Zhang, X.Y. Wang, L.L. Zheng, X.Y. Jiang, Studies of splat morphology and rapid solidification during thermal spraying, Int. J. Heat Mass Transf. 44 (2001) 4579–4592.

[26] M. Vardelle, A. Vardelle, A.C. Leger, P. Fauchais, D. Gobin, Influence of particle parameters at impact on splat formation and solidification in plasma spraying processes, J. Therm. Spray Technol. 4 (1995) 50–58.

[27] J.U. Brackbill, D.B. Kothe, C. Zemach, A continuum method for modeling surface tension, J. Comput. Phys. 100 (1992) 335–354.

[28] I.P. Gulyaev, O.P. Solonenko, P.Yu. Gulyaev, A.V. Smirnov, Hydrodynamic features of the impact of a hollow spherical drop on a flat surface, Tech. Phys. Lett. 35, 885 (2009).

[29] K. Shinoda, M. Raessi, J. Mostaghimi, T. Yoshida, H. Murakami, Effect of Substrate Concave Pattern on Splat Formation of Yttria-Stabilized Zirconia in Atmospheric Plasma Spraying, J. Therm. Spray Technol. 18 (2009) 609.

[30] H. Tabbara, S. Gu, Numerical study of semi-molten droplet impingement, Appl. Phys. A: Mater. Sci. Process. 104 (2011) 1011.s

Nomenclature

$\vec{x}$	Position vector
C	Specific heat ($kJkg^{-1}K^{-1}$)
f_l	Fraction of liquid
F	Volume of Fluid function
$\vec{g}$	Acceleration due to gravity (ms^{-2})
H	Latent enthalpy content of a control volume (Jkg^{-1})
Δt	Time step
K	Thermal conductivity ($Wm^{-1}K^{-1}$)
L	Latent heat of fusion (Jkg^{-1})
p	Pressure (Nm^{-2})
S	Source term

T	Temperature (K)
t	Time (s)
u	x component of velocity (ms^{-1})
v	y component of velocity (ms^{-1})
$\vec{u}$	Continuum velocity vector (ms^{-1})
x, y	Co-ordinates
Re	Reynolds number
ΔV	Volume of a computational

Greek symbols

□	Thermal diffusivity ($m^{-2}s$)
λ	Relaxation factor
μ	Dynamic viscosity (Nsm^{-2})
□	Kinematic viscosity (m^2s^-1)
ρ	Density (kgm^{-3})
▪	Surface tension coefficient
▬	Local mean curvature

Subscripts

d	Droplet
l	Liquid phase
n	Iteration level
m	Evaluated at melting point
p	Related to the grid point ‘P’
s	Solid phase
x	X component
y	Y component
eff	Effective
h	Enthalpy